Check for updates

Ultrafast dynamics of the UV-induced electronic relaxation in DNA guanine–thymine dinucleotides: from the Franck–Condon states to the minima of the potential energy surfaces

Vasilis Petropoulos, [a] Lara Martinez-Fernandez,*[b] Lorenzo Uboldi, [a] Margherita Maiuri, [a] Giulio Cerullo, *[ac] Evangelos Balanikas [d] and Dimitra Markovitsi *[e]

We study the DNA dinucleotide 5′-dGpdT-3′ (abbreviated as **GT**) as a model system for the relaxation of the electronic excited states in stacked nucleobases. Quantum chemistry calculations determine the Franck–Condon states and follow their evolution along the potential energy surfaces of the two most stable conformers. Three minima, corresponding to an excited charge transfer (^1CT) state, a $^1\pi\pi^*$ state located on the guanine moiety and a $^1n\pi^*$ state on the thymine moiety, are identified. Their spectral features are detected in the transient absorption spectra (*TAS*) recorded for buffered aqueous solutions between 330 and 650 nm with a time-resolution of 30 fs upon excitation at 266 nm. The striking difference between the *TAS* obtained for **GT** and an equimolar mixture of the corresponding mononucleosides indicates that the nucleobases are stacked in the majority of the dinucleotide molecules. The ^1CT state, in which a charge of 0.8 a.u. is transferred from the guanine to the thymine, is stabilized within 120 fs. The comparison of the **GT** behaviour with that of 5′-dTpdG-3′, characterized by an opposite polarity and studied previously by the same methodology, reveals that, when the guanine is positioned at the 5′ end, the lifetime of the $G^+ \rightarrow T^-$ ^1CT state is longer and the corresponding quantum yield higher.

1. Introduction

From the very first studies on the DNA photophysics and photochemistry, dinucleotides have been considered as convenient model systems for disentangling the excited state interaction among nucleobases.[1,2] Thus, the excimer/exciplex bands observed in their fluorescence spectra by Wilson and Callis,[3,4] half a century ago, were attributed to "charge resonance" excited states. Subsequent theoretical studies have characterized these excited states, referred currently as charge transfer (*CT*) states; they evidenced their formation during the electronic relaxation in such systems,[5–10] and computed the amount of the atomic charge that is transferred from one nucleobase to the other. Moreover,

ultrafast transient absorption (*TA*) experiments demonstrated that the population of ^1CT states constitutes an important pathway for the electronic relaxation;[11–15] and their lifetimes (τ_{CT}), determined for various pairs of nucleobases, were found to vary from a few ps to a few hundreds of ps.

While the dynamics of the backward charge transfer process, leading from the ^1CT to the ground state, is well characterized,[11–15] little is known about the forward process leading from the Franck–Condon state to the corresponding minimum (min-*CT*) of the potential energy surface (*PES*). This type of study requires not only an exceptionally high time resolution but also broad spectral coverage, so as to identify properly the related spectral signatures. Their rationalization through computations may help disentangle them from other relaxation paths. We applied recently such a methodology to the study of three dinucleoside monophosphates, 5′-dTpdG-3′, 5′-dApdG-3′ and 5′-dGpdA-3′, for simplicity called hereafter "dinucleotides" and abbreviated as **TG**, **AG** and **GA**, respectively; in all these systems, we observed that, following excitation at 266 nm, the ^1CT states are fully formed within 100–130 fs.[16,17]

Another issue that emerged from our recent studies is the role of the DNA polarity (also called directionality),[15,17] that is the order according to which the nucleobases are linked

a Dipartimento di Fisica, Politecnico di Milano, Piazza Leonardo da Vinci 32, I-20133 Milano, Italy. E-mail: giulio.cerullo@polimi.it

b Departamento de Química Física de Materiales, Instituto de Química Física Blas Cabrera, Consejo Superior de Investigaciones Científicas, IQF-CSIC, Calle Serrano 119, 28006 Madrid, Spain. E-mail: lmartinez@iqf.csic.es

c Istituto di Fotonica e Nanotecnologie-CNR, Piazza Leonardo da Vinci 32, I-20133 Milano, Italy

d Laboratoire d'Optique et Biosciences, Ecole Polytechnique, CNRS-INSERM, Institut Polytechnique de Paris, 91120 Palaiseau, France

e Université Paris-Saclay, CNRS, Institut de Chimie Physique, UMR 8000, 91405 Orsay, France. E-mail: dimitra.markovitsi@universite-paris-saclay.fr
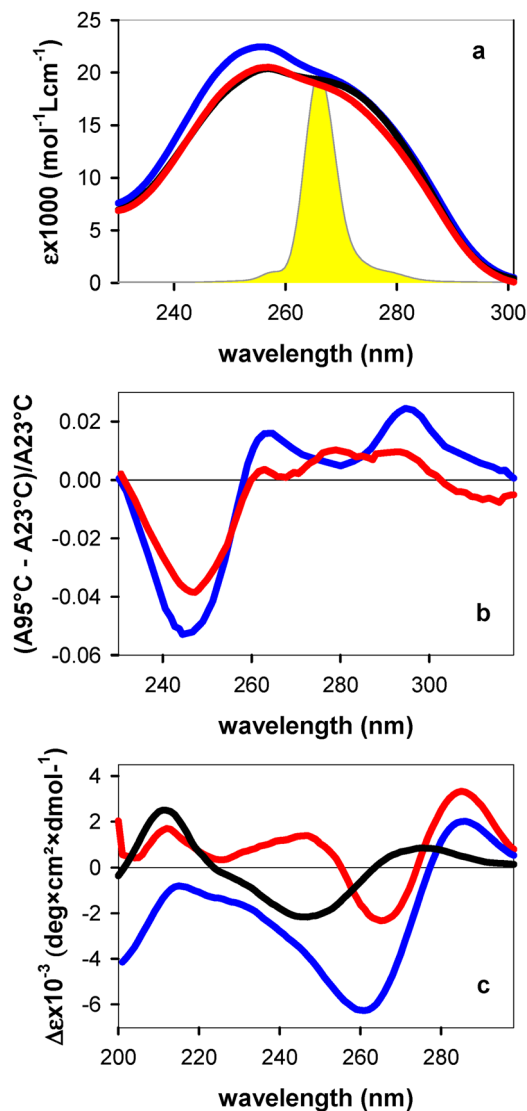
14936 | *Phys. Chem. Chem. Phys.*, 2025, **27**, 14936–14947

This journal is © the Owner Societies 2025

Paper

PCCP

Fig. 1 Comparison of the steady-state absorption (a), thermal (b) and CD spectra (c) of **GT** (red) and **TG** (blue) and an equimolar mixture of dG and dT (black). In (a) the absorbance is normalized at 266 nm, corresponding to the peak intensity of the exciting laser pulse (yellow). The thermal spectra are the difference between the steady-state absorption spectra recorded for each dinucleotide at 95 °C (A95 °C) and 23 °C (A23 °C), divided by A23 °C.

together *via* the phosphodiester backbone from the 5′ end to the 3′ end.[18] The latter is known to control the conformations adopted by nucleic acids,[19–21] and to play a key role in biological functions depending on structural features.[22–25] Its influence on redox reactions,[26–29] hole transport[30] and charge recombination[31] in DNA as well as on the photoionization of guanine quadruplexes[32] was highlighted. Although several years ago computational studies predicted its effect on the Franck–Condon states of stacked nucleobases,[33,34] our understanding of the way the DNA polarity affects the excited state relaxation remains poor. So far, only one pair of nucleosides with opposite polarity, **AG**/**GA**, was studied by time-resolved spectroscopy.[14,15,17]

Within the above-described context, here we focus on the 5′-dGpdT-3′ dinucleotide, called **GT** in the following, using the

previously applied experimental and computational methodology.[16,17] We record its *TA* spectra (*TAS*) from 330 to 650 nm with a time resolution of 30 fs upon 266 nm excitation. In parallel, using quantum chemistry calculations, we determine the most stable ground state conformations with stacked nucleobases, we compute the excited states underlying the steady-state absorption spectrum of **GT** and follow their evolution along the corresponding *PES*. Moreover, we calculate the *TAS* of both the Franck–Condon states and the optimized excited minima. We interpret our experimental data in the light of the qualitative information provided by our computations and the experimental data obtained for the monomeric chromophores, 2′-deoxyguanosine (dG) and thymidine (dT). Finally, we parallel our conclusions with those derived from a quantitative analysis using global fits with exponential functions, which, however, fails to grasp the complexity of the processes.

Our work has two main objectives. First, to shed further light on the UV-induced processes taking place in **GT**, whose relaxation pathways were studied previously[13,14] with lower time resolution and without theoretical support regarding the relaxation pathways. Second, to enrich our understanding of the effect of the strand directionality, comparing the behaviour, on the one hand, of the **GT** with that of **TG**, and, on the other hand, that of the **GT**/**TG** pair with the **GA**/**AG** pair, all of them studied following the same methodology.[16,17]

2. Experimental results

2.1 Steady-state spectra

Fig. 1 shows the steady-state properties of **GT**, **TG**, and an equimolar mixture of the mononucleosides. To avoid aggregation, the monomeric chromophores were dissolved in pure water instead of the phosphate buffer (120 mM) used for the dinucleotides.

The absorption spectra (Fig. 1a) exhibit only small differences: the intensity of the peak located at ∼257 nm is lower for **GT** compared to **TG**. Greater differences are encountered in the "thermal spectra", which reflect the percentage changes in the absorbance observed upon heating to high temperature, where base stacking is destroyed (see for example Fig. 4 in ref. 35). Those of **GT** and **TG**, determined as the difference between the steady-state absorption spectra recorded for each dinucleotide at 95 °C (A95 °C) and 23 °C (A23 °C) and divided by A23 °C, are shown in Fig. 1b. Both of them reveal hyperchromic and hypochromic effects, which are typical of base stacking. The pattern observed for **GT** is richer, with three positive and two negative peaks, compared to that of **TG**, characterized by only one negative and two positive peaks, albeit with larger amplitudes. Finally, the circular dichroism (CD) spectrum of **GT** differs from those of **TG** and the monomer mixture (Fig. 1c). It is characterized by maxima at 247 and 285 nm and minima at 212 and 265 nm.

2.2 Time resolved data

The contour 2D maps and the *TAS* recorded for **GT** and an equimolar mixture of dG and dT upon impulsive photoexcitation at 266 nm are presented, respectively, in Fig. 2 and 3. We
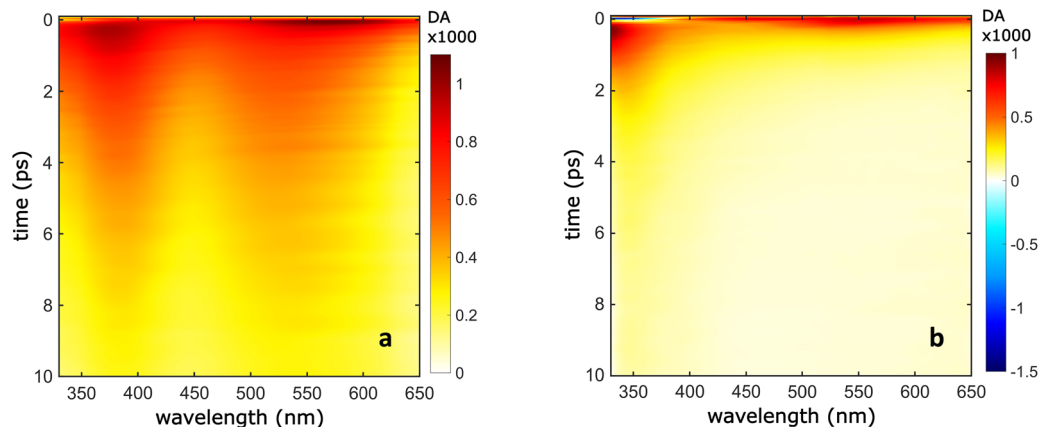
This journal is © the Owner Societies 2025

Phys. Chem. Chem. Phys., 2025, **27**, 14936–14947 | **14937**

Fig. 2   Contour 2D maps recorded for **GT** (a) and an equimolar mixture of dG and dT (b) with excitation at 266 nm.
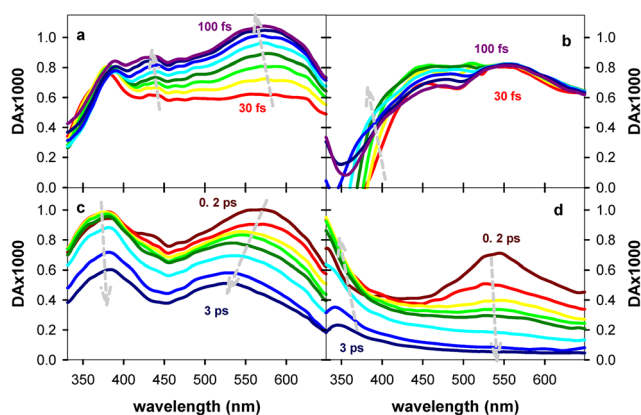

Fig. 3   *TAS* recorded for **GT** (a) and (c) and an equimolar mixture of dG and dT (b) and (d). (a) and (b) From 30 fs to 100 fs with 10 fs steps; (c) and (d) at 0.2 ps (dark red), 0.3 ps (red), 0.4 ps (yellow), 0.5 ps (light green), 0.6 ps (dark green), 1.0 ps (cyan), 2.0 ps (blue) and 3.0 ps (dark blue).

Fig. 4   Comparison of the *TA* signals recorded for **GT** (red), **TG** (blue) and an equimolar mixture of dG and dT (black) at 570 nm for early times (a) and 530 nm for longer times (b). The instrumental response function is shown in yellow (a). Green lines in (b) correspond to fits with mono-exponential functions.

note that the molar absorption coefficient at 266 nm is similar for the two nucleosides;[36] therefore, they have the same probability to be excited by our laser pulses. We also stress that in these experiments the dinucleotide concentration (4×10^{-3} mol L^{-1}) was much higher than the concentration of absorbed photons per pulse (8×10^{-6} mol L^{-1}), rendering their two-photon ionization improbable.

Between 30 and 100 fs, the **GT** *TAS* (Fig. 3a) do not exhibit significant changes below 380 nm. At longer wavelengths, a small band at $\sim$445 nm and a more intense one located around 570 nm are growing rapidly. A completely different picture is observed in the case of the monomers (Fig. 3b): no evolution in the red part of the *TAS*, while in the blue part, the differential absorbance (DA), initially negative, starts acquiring positive values only after 90 fs. The negative DA signal at early times is due to the stimulated emission of the thymidine chromophore, already reported in the literature.[13,37]

On longer times, the small band at 445 nm disappears from the **GT** *TAS* (Fig. 3c), while the long-wavelength band shifts from 570 nm to 530 nm at 3 ps. At that time a second band, peaking at 379 nm and exhibiting a small shoulder at shorter wavelengths, is
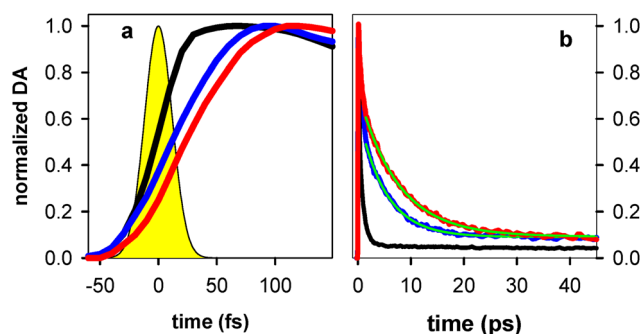
also present in the *TAS*. In the case of the monomers (Fig. 3d), the peak at 550 nm present at 0.2 ps decays rapidly; the main feature at 3 ps is a weak photoinduced absorption peak at 355 nm.

The **TG** *TAS*,[16] although not identical to those of **GT**, present important similarities. In particular, a band is growing rapidly at long wavelengths and shifts to shorter ones, before decaying completely. The dynamics of these processes are compared in Fig. 4. At early times, the rise of the *TA* signal at 570 nm is completed within 120 fs for **GT** *vs.* 90 fs for **TG** (Fig. 4a). We also observe that the rise of the signal corresponding to an equimolar mixture of mononucleotides is much faster, following the temporal profile of the instrumental response. In later times, the decay of the band at 530 nm is slower for **GT** than for **TG** (Fig. 4b). The time constants derived from fits with mono-exponential functions, starting at 1.5 ps, when the contribution from the bright states of nucleobases has practically disappeared,[38] are, respectively, 7.48 ± 0.06 ps and 5.44 ± 0.03 ps.

2.3   Global fits

A usual way of analysing *TA* data on DNA is to perform fits with multi-exponential functions and assign the derived time constants to specific excited states. In a previous study, the *TA*
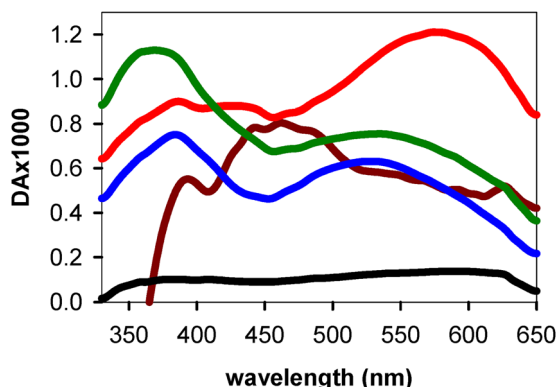
14938 | *Phys. Chem. Chem. Phys.*, 2025, **27**, 14936–14947

This journal is © the Owner Societies 2025

Fig. 5 *EAS* obtained through a global fit of the **GT** *TAS* with five exponential functions. Associated time constants: τ_1 = 60 fs (dark red), τ_2 = 320 fs (red), τ_3 = 0.7 ps (green), τ_4 = 7.0 ps (blue) and τ_5 = >1 ns (black). The negative signal in the 60-fs *EAS* arises from the coherent artifact.

signal recorded for **GT** with a time resolution of $\sim$150 fs at 380 nm upon 257 nm excitation, yielded three time constants: τ_1 = 3 ± 2 ps, τ_2 = 9 ± 7 ps and τ_3 = >1 ns, attributed, respectively, to the monomeric $^1\pi\pi^*$ states, the ^1CT state and the thymine triplet state.[13]

We performed a global analysis of the *TAS* of **GT**, which required five exponential components in order to obtain an acceptable fit. The derived time constants are: τ_1 = 60 fs, τ_2 = 320 fs, τ_3 = 0.7 ps, τ_4 = 7.0 ps and τ_5 = >1 ns; the corresponding evolution associated spectra (*EAS*) are reported in Fig. 5. In agreement with the previous study,[13] we found a long (τ_5 > 1 ns) component and τ_4 could be associated with the ^1CT state. But no further information can be extracted. We note that five time constants (120 fs, 250 fs, 800 fs, 2.1 ps and 2 ns) are needed to fit the data obtained for the dG and dT equimolar mixture under the same conditions.[16]

3. Theoretical results

3.1 Ground state structure

We optimized the ground state geometry of **GT** considering the main four possible stacking modes: *anti–anti*, *anti–syn*, *syn–anti* and *syn–syn*. The notations *anti* and *syn* refer to the position of each nucleobase, in the order 5′ to 3′, with respect to the angle of the glycosidic bond associated with the deoxyribose moiety. Their energies ΔE were computed taking as a reference that of the *anti–anti* one, encountered in B-form double strands. They are found to be, respectively, 0.00, 0.01, 0.09 and 0.25 eV. Although the lowest energy is found for the *anti–anti* conformer, the difference with the *anti–syn* one is only 0.01 eV. Therefore, both of them are expected to be present at room temperature, where the energy of thermal fluctuations is 0.025 eV.

The structures of the two most stable conformers, whose excited state properties will be examined in detail hereafter, are shown in Fig. 6a. The difference in their geometry is reflected in their CD spectra (Fig. 6b). A straightforward comparison between theoretical and CD experimental spectra is delicate *per se*, and *a fortiori* when more than one conformer are present. However, we observe that the pattern of the spectrum in Fig. 1c resembles more that computed for the *anti–anti* conformer: starting from the long wavelengths, there is an alternation of a maximum, a minimum, a maximum and finally a minimum. Such similarity is in line with the finding that the *anti–anti* conformer is the most stable one, and, consequently, it is expected to be more abundant in the solution.

3.2 Franck–Condon states and their relaxation

The properties of the 5 lowest in energy Franck–Condon excited states of *anti–anti* **GT** and *anti–syn* **GT** are shown in Table 1.
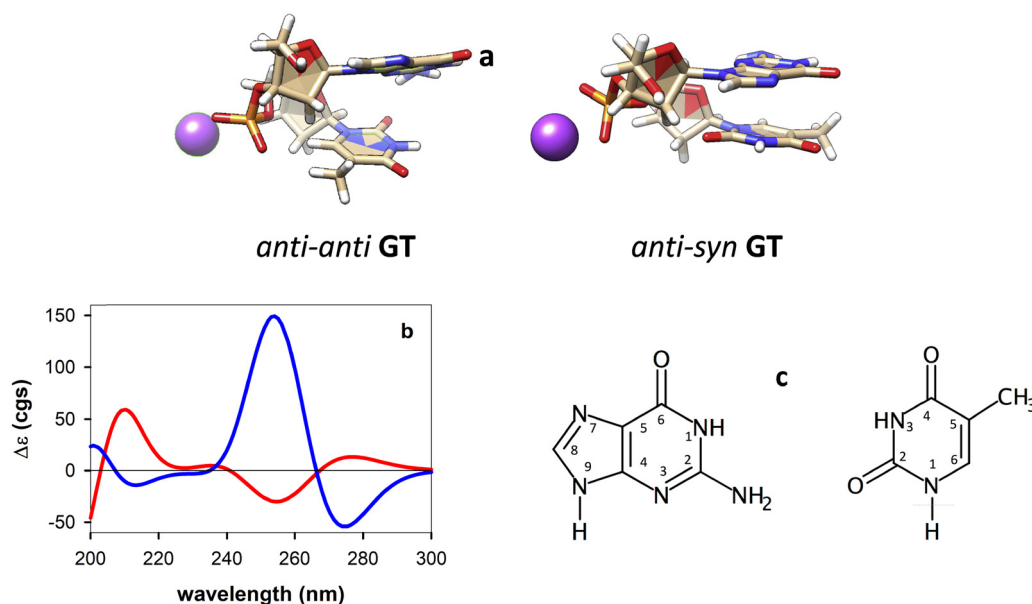

Fig. 6 Ground state structure of the two most stable **GT** conformers (a) and associated CD spectra (b); *anti–anti* (red); *anti–syn* (blue). (c) Atom labelling for guanine and thymine.

This journal is © the Owner Societies 2025

Phys. Chem. Chem. Phys., 2025, **27**, 14936–14947 | **14939**

Table 1 Properties of the Franck–Condon states determined for the two most stable conformers of **GT** at the PCM/M052X/6-31G(d) level of theory. VAE: vertical absorption energy; f: oscillator strength; δ: charge transfer character

State	Character	VAE (eV)	f	δ (a.u.)
anti–anti **GT**				
S_1	$n\pi^*T$	5.16	0.001	0.0
S_2	$\pi\pi^*G(La)$	5.33	0.144	0.0
S_3	$\pi\pi^*T + G^+ \to T^-\ CT$	5.40	0.251	0.1
S_4	$G^+ \to T^-\ CT$	5.60	0.048	0.8
S_5	$n\pi^*G$	5.65	0.002	0.0
anti–syn **GT**				
S_1	$n\pi^*T$	5.18	0.000	0.0
S_2	$\pi\pi^*G(La) + G^+ \to T^-\ CT$	5.28	0.057	0.2
S_3	$\pi\pi^*G(La) + G^+ \to T^-\ CT$	5.40	0.165	0.4
S_4	$\pi\pi^*T + G^+ \to T^-\ CT$	5.49	0.215	0.2
S_5	$n\pi^*G$	5.64	0.002	0.0

Those of *anti–anti* **GT** had already been already reported in ref. 32, but for comparison reasons, we present them again.

For both systems, S_1 and S_5 are dark, $^1n\pi^*T$ and $^1n\pi^*G$, respectively, while S_2, S_3 and S_4 carry significant oscillator strength and can be excited by the laser pulses. Yet, the nature of these "excitable" states is not the same for each conformer. For *anti–anti* **GT**, we have, in the order, a $^1\pi\pi^*G(La)$, a $^1\pi\pi^*T$ with a small CT character (0.1 a.u.) and a $^1G^+ \to T^-\ ^1CT$ (0.8 a.u.). In the case of *anti–syn* **GT**, the coupling between ^1CT and $^1\pi\pi^*$ states is more important, giving rise to mixed states: S_2 (0.2 a.u.) and S_3 (0.4 a.u.) involving the $^1\pi\pi^*G(La)$ state, and S_4 (0.2 a.u.) involving the $^1\pi\pi^*T$ state.

Fig. 7 shows the individual spectra of the electronic transitions composing the steady-state absorption spectra of the two conformers together with the exciting laser pulse. A Gaussian width of 0.4 eV (FWHM) was applied to each transition, which was shifted by −0.65 eV. The latter value was chosen so that the energy computed by the same methodology for the $^1\pi\pi^*(La)$ state of dG in water coincides with the position of this transition in the experimental spectra.[39] Fig. 7 is not intended to convey quantitative information regarding the percentage contribution of each Franck–Condon state to the overall excited state population. It simply illustrates in a qualitative way which states are likely to be populated and establishes the connection, *via* a colour code, with the minima reached following evolution of each one of them.

The properties of the minima in the *PES* corresponding to each one of the above considered Franck–Condon states are shown in Table 2, where are also noted the main structural changes accompanying the relaxation paths. Overall, 3 different types of minima were identified: min-$^1\pi\pi^*G(La)$ and min-^1CT stemming from both conformers, and $^1n\pi^*T$ originating mainly from the *anti–syn* **GT**, in the sense that it results from an "excitable" Franck–Condon state. In the case of *anti–anti* **GT**, S_3 arrives to a degeneracy between $^1\pi\pi^*T$ and S_0 states while S_5 arrives to a degeneracy region between $^1n\pi^*G$ and S_0 states without reaching any minimum.

3.3 Computed *TAS*

The spectral changes expected upon relaxation of the Franck–Condon states toward the corresponding min-^1CT are shown in
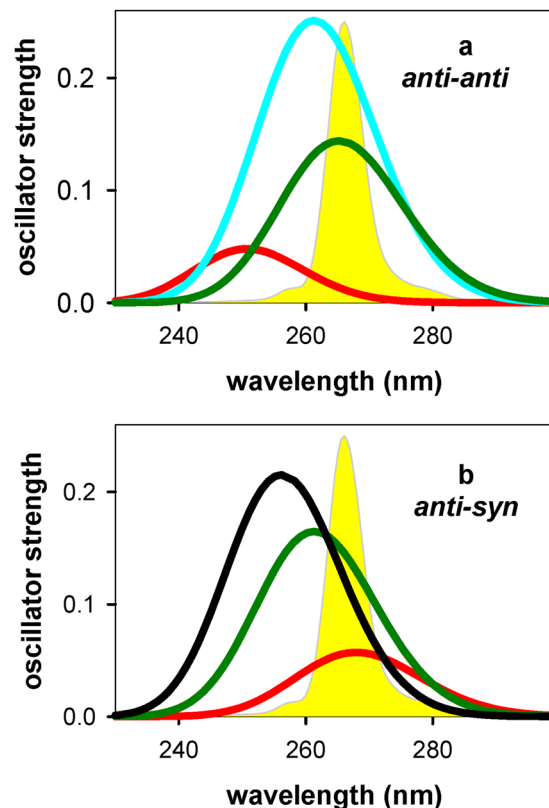

Fig. 7 Individual transitions (Table 1) composing the steady-state absorption spectrum of *anti–anti* **GT** (a) and *anti–syn* **GT** (b); the colour code is defined by the minimum toward which each Franck–Condon state evolves (Table 2): min-^1CT (red); min-$^1\pi\pi^*G(La)$ (green); ground state (cyan); min-$^1n\pi^*T$ (black); in yellow: spectrum of the exciting laser pulse.

Fig. 8. We focus on S_4 for *anti–anti* **GT** and S_2 for *anti–syn* **GT**, which are the most likely to be populated by the exciting laser pulse. The *TAS* of both min-^1CT present a band in the UV and a second one in the 500–600 nm range. Moreover, their formation results in an intensity increase. But an important difference between the two conformers is that population of

Table 2 Properties of the minima located on the *PES* of the first excited state determined for the two most stable conformers of **GT** at the PCM/M052X/6-31G(d) level of theory.[32] ADE: adiabatic (with respect to the S_0 at the Franck–Condon region) energies; VEE: vertical (with respect to the S_0 at the corresponding minimum) emission energies; f: oscillator strength; δ: charge transfer character; initial state optimized and main reaction coordinate

Minima	ADE (eV)	VEE (eV)	f	Initial state	Reaction coordinate[a]
anti–anti **GT**					
$^1\pi\pi^*G(La)$	4.51	2.08	0.019	S_2	C1–C2–NH2
^1CT	4.27	3.23	0.023	S_4	Interbase distance
$^1n\pi^*T$	4.76	3.70	0.001	S_1	Out of plane O4
anti–syn **GT**					
$^1\pi\pi^*G(La)$	4.71	2.40	0.024	S_3	C1–C2–NH2
^1CT	4.44	3.40	0.011	S_2, S_5	Interbase distance
$^1n\pi^*T$	4.76	3.79	0.001	S_1, S_4	Out of plane O4

^{a} The atom labelling is shown in Fig. 6c.

14940 | *Phys. Chem. Chem. Phys.*, 2025, **27**, 14936–14947

This journal is © the Owner Societies 2025
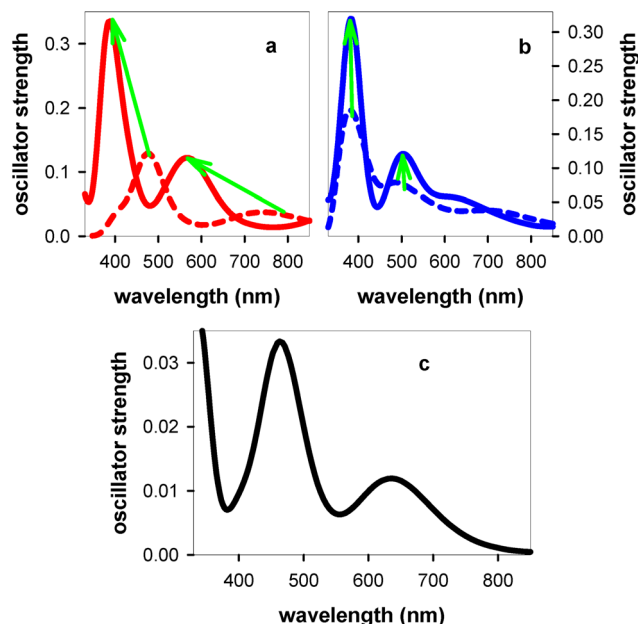
Fig. 8 *TAS* computed for min-^1CT (solid lines) of *anti–anti* **GT** (a), *anti–syn* **GT** (b) and the min-^{1}nπ*T of *anti–syn* **GT** (c). Dashed lines correspond to the *TAS* of the initial Franck–Condon states, S_4 in (a) and S_2 in (b).

the min-^1CT in *anti–anti* **GT** induces a blue shift of the absorption band (Fig. 8a), while in the case of *anti–syn* **GT**, no significant change in the position of these two bands is noticed (Fig. 8b).
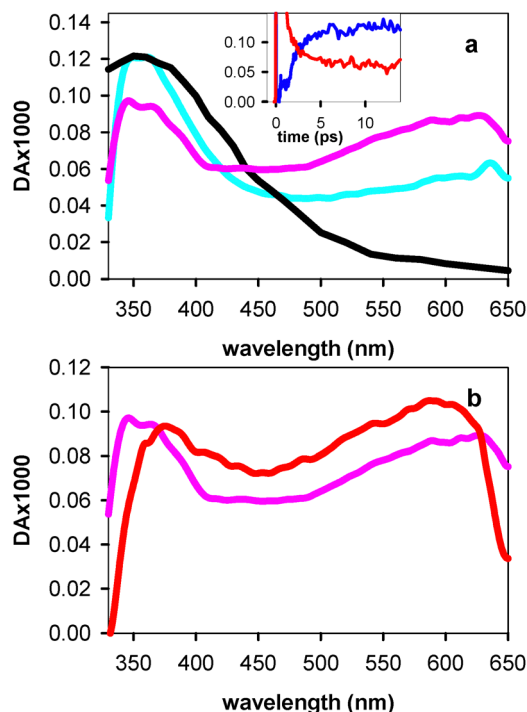

Fig. 9 (a) *TAS* recorded for dT at 2.5 ps (pink) and 40 ps (cyan); the TMP *TAS* recorded at 200 ns by ns *TA* spectroscopy following 266 nm excitation is shown in black.[48] Inset: *TA* signals of dT at 350 nm (blue) and 600 nm (red). (b) Comparison between the *TAS* of **GT** at 40 ps (red) and that of dT at 2.5 ps (pink).

The *TAS* of min-^{1}nπ*, expected to stem from *anti–syn* **GT**, is shown in Fig. 9a.

4. Discussion

4.1 Ground state

The striking difference observed below 100 fs between the *TAS* of **GT** and those of an equimolar mixture of dG and dT (Fig. 2 and 3a, b) show that (i) the nucleobases in the dinucleotide are largely coupled already in the ground state, and (ii) the relaxation pathways leading from the Franck–Condon states to the excited state minima are different compared to those of the monomeric chromophores. The ground state interaction is also attested by the different CD spectra recorded for **GT** and the monomer mixture (Fig. 1c). Moreover, the hypochromic and hyperchromic effects in the **GT** thermal spectrum (Fig. 1b), known to result from coupling between ^{1}ππ* and ^1CT transitions, which require orbital overlap, are indicative of base stacking.[40,41]

According to our quantum chemistry study, two conformers with stacked nucleobases, *anti–anti* and *anti–syn*, are likely to be present in the solution. The fact that the pattern of the experimental CD spectrum (Fig. 1c) resembles that computed for the former conformer (Fig. 6b) suggests that it represents the dominant conformation. Yet, the structure of the thermal spectrum (Fig. 1b), richer compared to that obtained for **TG**, for which a single conformer is expected in room temperature solutions,[16] indicates the absence of a unique conformation.

4.2 Assignment of the spectral evolution

One important reason for the difficulty to draw additional conclusions from the global fits presented in Fig. 5 is the complex excited state scenario, with the presence in the solution of two conformers and the population by the pump pulses of at least three Franck–Condon states for each one of them (Fig. 7), and, possibly, of a small fraction of unstacked chromophores. Another constraint comes from the fact that we start probing at very short times, when evolution along *PES*, which are low-dimensional spaces, still takes place. Therefore, exponential dynamics, valid when the interactions of the chromophore with its environment are uniform in the three-dimensional space, do not correctly describe the involved processes.[42] In low-dimensional spaces dynamical patterns may be given, for example, by stretched exponentials or power-law functions.[43–45] Theoretical models addressing this question for bichromophoric molecules characterized by many degrees of freedom have not yet been developed.

Given these obstacles, we propose below a rather semi-quantitative assignment based on the results of our computations providing mainly "characteristic times" instead of time constants.

4.3 The ^{1}nπ* state

As mentioned in Section 2.3, our global fit on **GT** revealed the presence of a transient species too long to be correctly determined by probing only over the first 40 ps. Duchi *et al.* had

This journal is © the Owner Societies 2025

Phys. Chem. Chem. Phys., 2025, **27**, 14936–14947 | **14941**

equally found a long-lived transient for **GT** and assigned it to the triplet state of the thymidine chromophore.[13] Therefore, we first discuss the behaviour of monomeric thymidine and then we compare it with that of the dinucleotide.

The triplet state of the thymidine chromophore was detected 60 years ago.[46,47] Its spectral and dynamical features were determined later with better precision by ns *TA* spectroscopy for oxygen-free solutions.[48,49] Recent studies assigned it to the $^3\pi\pi^*$ state, which is formed from the $^1n\pi^*$.[50,51] This picture is confirmed by our measurements on dT. The dT *TAS* at 40 ps closely resembles that of the triplet state (Fig. 9a) determined for thymidine monophosphate (TMP) at 200 ns;[48] the slightly stronger intensity (by DA $\approx 5 \times 10^{-5}$) at long wavelengths is due to a weak contribution of hydrated electrons[52] stemming from two-photon ionization of the buffer. This transient is formed within ~ 10 ps (inset in Fig. 9a), in line with a previous study.[53] Therefore, the *TAS* at 2.5 ps, exhibiting a relatively higher intensity around 600 nm, corresponds to the $^1n\pi^*$ (Fig. 9a). We have not detected the formation of the second long-lived transient observed by Pilles *et al.* and assigned to an unknown species X.[50] A recent paper by Suzuki and co-workers[54] evidenced that this transient corresponds to a ground state intermediate, detected at 300 nm, which falls outside the spectral area probed in our experiments.

The **GT** *TAS* at 40 ps clearly differs from that of dT at 40 ps, but matches better the one at 2.5 ps (Fig. 9b) associated with the $^1n\pi^*$ state. This is consistent with our calculations on **GT**, which identified a min-$^1n\pi^*$T. It should mainly originate from the S_4 state of the *anti–syn* conformer (Fig. 7b). Although the S_1 state of the *anti–anti* conformer also evolves toward the same minimum, its oscillator strength is so weak (0.001) that it is negligibly populated by the exciting laser pulse. In addition, the *TAS* computed for min-$^1n\pi^*$ is characterized by two absorption bands (Fig. 8c) as observed for the long-lived transient of **GT** and the $^1n\pi^*$ state of dT (Fig. 9b). Therefore, we conclude that this transient corresponds to the $^1n\pi^*$T and not to the $^3\pi\pi^*$T state.

Finally, it is worth-noting that a long-lived transient with similar spectral features was also detected for **TG**.[16] And also in that case, a min-$^1n\pi^*$T was identified theoretically.

4.4 The ^1CT state

The *EAS* associated with the time constant of 7.0 ps (Fig. 5) certainly contains the fingerprint of the ^1CT state, already identified by time-resolved infrared spectroscopy.[13,14] Yet, it is highly probable that this time constant also embodies the long component of the guanosine $^1\pi\pi^*$ state absorbing in the UV, whose lifetimes reported in the literature fall in the range 1.9–2.7 ps.[55–59] An indication for such a superposition appears in the fits of individual decays with mono-exponential functions between 1.5 and 45 ps. Although the obtained R^2 values are higher than 0.99, the resulting time constants decrease when moving from the visible toward the UV. For example, it is 7.48 ± 0.06 ps at 530 nm (Fig. 4b) and only 6.04 ± 0.01 ps at 380 nm. Following this reasoning, we judge that the value of 7.48 ps, determined by tail fitting starting at 1.5 ps, is reliable since it is determined for wavelengths longer than 500 nm, a range in
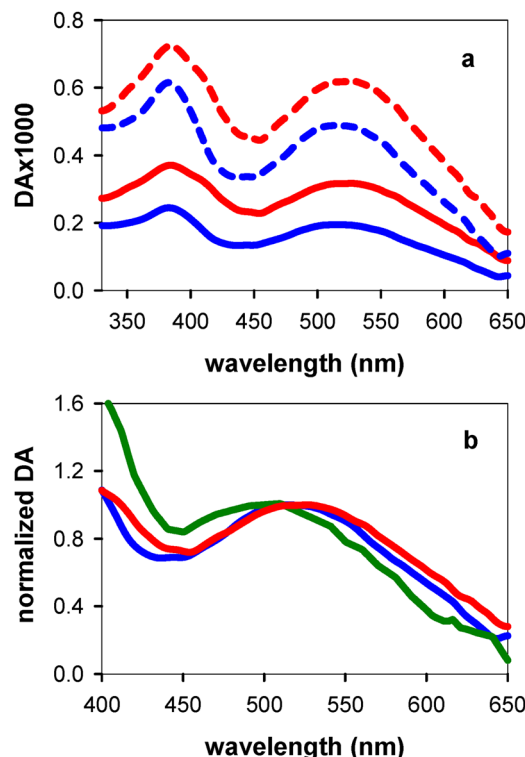

Fig. 10 (a) *TAS* of the ^1CT states (solid lines) at 5 ps of **GT** (red) and **TG** (blue) determined after subtraction of the corresponding *TAS* of the $^1n\pi^*$ at 40 ps; dashed lines are derived from the ^1CT *TAS* at 5 ps extrapolated to "zero time" taking into account their lifetime (for more explanations see text). (b) Comparison of the spectral profiles of the ^1CT *TAS* with the sum of the spectra of the guanosine radical cation[60] and the thymidine radical anion;[61] intensities are normalized to the maximum at the long wavelength band.

which the contribution of the bright monomer states has become negligible. This value is slightly lower than those reported in previous studies, ~ 10 ps[13] and 14 ± 5 ps.[14]

In order to better characterize the spectrum of the ^1CT state, we subtracted the **GT** *TAS* at 40 ps, already assigned to the $^1n\pi^*$T state, from the *TAS* at 5 ps, when the monomer contribution has already decayed. The resulting difference is compared to that corresponding to **TG**: in Fig. 10a the two spectra are shown with their DA, while in Fig. 10b, focusing on the visible spectral domain, their intensity is normalized at the maximum of the band, peaking at 526 nm for **GT** and 514 nm for **TG**. Both bands largely overlap with that corresponding to the sum of the spectra of guanosine radical cation and the thymidine radical anion, determined, respectively, by flash photolysis[60] and pulse radiolysis.[61] This similarity further supports the assignment of this transient species to a $G^+ \rightarrow T^-$ ^1CT state.

Our computations showed that a min-^1CT can be reached in both **GT** conformers, but no trace of a second ^1CT state could be found in our experimental data. This is understandable because the spectral features of the two min-^1CT are quite similar (Fig. 8).

Having discussed the properties of min-*CT* based on the ps *TA* data, we turn to shorter times, searching the dynamics of its

14942 | *Phys. Chem. Chem. Phys.*, 2025, **27**, 14936–14947

This journal is © the Owner Societies 2025

formation from the Franck–Condon states. Again, we focus on the long wavelengths, where a band is growing in the **GT** *TAS*, while no change is observed in the case of the equimolar mixture of dG and dT (Fig. 2a and b). Our computations predict that, for both conformers, the intensity of all the bands present in the *TAS* of min-^1CT is higher than that of the corresponding Franck–Condon state (Fig. 8). This growth is completed within 120 fs, as attested by the rise of the *TA* signal at 570 nm (Fig. 4a). During this time interval, the peak intensity increases by 75% but no clear trend is observed regarding its position; the 30 fs *TAS* is rather flat and, subsequently, the position of the maximum varies between 569 and 578 nm.

In comparison, the rise of the **TG** at 570 nm is somewhat faster, being completed within 100 fs, the increase of the peak intensity is smaller (47%) and the maximum of the band is progressively blue-shifted by 25 nm.[16] A somewhat slower formation (130 fs) of the ^1CT state was also found for **AG** compared with **GA** (110 fs).[17] It is worth-noting that for both pairs, the slower process is observed for the dinucleotide for which two conformers exist in solution (**GT** and **AG**).

Based on the *TAS* in Fig. 10a, representing the *TA* of the ^1CT states at 5 ps, and the corresponding lifetimes determined for **GT** (7.48 ps) and **TG** (5.44 ps), we determined their "zero-time" spectra, also shown in Fig. 10a as dashed lines. To this end, we used the equation $(DA)_0 = (DA)_{5ps}/\exp(-5/\tau_{CT})$. It appears that the zero-time *TAS* of **GT** is significantly more intense than that of **TG**; the difference amounts to 25% for the peak in the visible and is indicative of the relative quantum yield of the formation of the ^1CT state (Φ_{CT}) within each system. This can be explained by the stability of the corresponding min-^1CT: its energy both in *anti–anti* **GT** and *anti–syn* **GT** is lower than that of min-$^1\pi\pi^*$G(La) by 0.24 eV and 0.27 eV, respectively (ADE in Table 2), thus precluding further transformation towards a lower-lying minimum. The opposite situation is encountered for **TG**, where the min-$^1\pi\pi^*$G(La) is more stable by 0.14 eV compared to min-^1CT.[16]

From the $(DA)_0$ values, it is possible to get a rough evaluation of Φ_{CT} using the molar absorption coefficient of an equimolar mixture of the dT radical anion and the dG radical cation (990 mol^{-1} L cm^{-1}) and considering the concentration of absorbed photons (8×10^{-6} mol L^{-1}). In this way, we obtain 0.78 for **GT** and 0.62 for **TG**. These are rather high values which should be considered as upper limits for Φ_{CT}, because the molar absorption coefficient is expected to be higher for the CT states, in which the charge transferred between the two nucleobases is only 0.8 a.u.[17] However, despite the numerous approximations in this evaluation, it is clear that the values of the **GT**/**TG** pair are much higher than those determined previously for the **GA**/**AG** pair (0.32/0.18), following exactly the same procedure (Table 3). It is worth noting that Kufner *et al.* reported a similar trend: the Φ_{CT} values, estimated from their transient infrared signals, are 0.66 ± 0.35 for **GT**, 0.42 ± 0.20 for **GA** and 0.32 ± 0.15 for **AG**.[14]

4.5 The $^1\pi\pi^*$ states

The fact that stimulated emission is absent from the **GT** *TAS* at early times (Fig. 3a) means that the percentage of unstacked

Table 3 Φ_{CT} values estimated for two pairs of dinucleotides with opposite polarity. $I_{max,0}$ is the maximum intensity of the long-wavelength band of the CT state at zero time. In parentheses, estimations reported in ref. 14

	GT	TG	GA	AG
$I_{max,0}$ ($\times 10^3$)	0.62	0.49	0.31[15]	0.21[15]
Φ_{CT}	0.78	0.62	0.32[15]	0.18[15]
	(0.66)[14]		(0.42)[14]	(0.32)[14]

thymine moieties behaving as "free" chromophores is very small. The $^1\pi\pi^*$T state is involved in Franck–Condon states of dinucleotides with stacked nucleobases: S_3 and S_4 of *anti–anti* **GT** and in S_4 of *anti–syn* **GT** (Table 1). However, all of them contain even a small part of CT and none evolves toward a min-$^1\pi\pi^*$T (Table 1).

The situation is different for $^1\pi\pi^*$G(La), which corresponds to the S_2 state of the *anti–anti* conformer evolving toward min-$^1\pi\pi^*$G(La). The same minimum is reached from the S_3 state of *anti–syn* **GT**, characterized by an important (0.4 a.u.) CT character.

We assign to $^1\pi\pi^*$G(La) the small band growing between 430–450 nm, also present in the dG *TAS*.[16] From 30 to 100 fs its intensity increases by 42% in a quasi-linear way (Fig. 11a). This rise is somewhat faster (100 fs *vs.* 120 fs) compared to that observed for the long wavelength band (Fig. 4a). A possible explanation could be that a more important structural modification takes place during the stabilization of min-^1CT compared to min-$^1\pi\pi^*$G(La). The former requires mutual motion of the two nucleobases, while the latter involves just the modification of an intra-base angle (Table 2). The *PES* leading from the $^1\pi\pi^*$(La) Franck–Condon state of the guanosine chromophore to the corresponding minimum is quite complex.[62] *TA* measurements showed that the red part of the *TAS* decays more rapidly than the UV part.[55,57–59] Thus, we reported in our previous study on **TG**, that above 500 nm the dG decay between 0.2 and 2 ps can be described with a mono-exponential function with a time constant of 0.6 ps, and we argued that this decay induces a blue shift of the long wavelength band following a similar dynamical pattern. The same blue shift is also observed in the case of **GT** (Fig. 3c). The position of the band maximum can be approximated with a mono-exponential function with a time constant of 0.5 ± 0.1 ps (Fig. 11b), which is close to that found for dG.
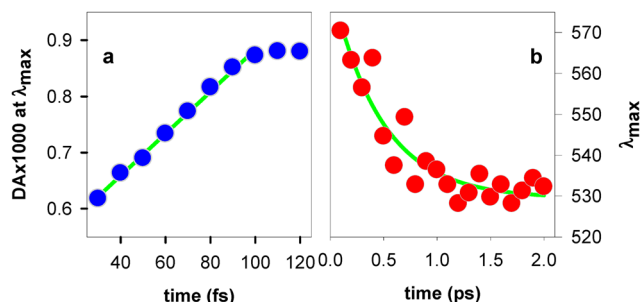

Fig. 11 Variation of the peak intensity at the 430–450 nm spectral domain (a) and position of the maximum of the long wavelength band (b) observed in the **GT** *TAS*. Green lines are fits with linear (a) and mono-exponential (b) functions.
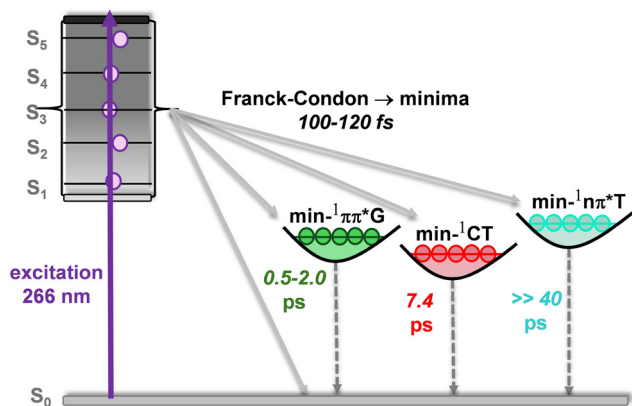
This journal is © the Owner Societies 2025

Phys. Chem. Chem. Phys., 2025, **27**, 14936–14947 | **14943**

Fig. 12 Simplified drawing of the Franck–Condon excited states and the corresponding minima computed in the *PES* of **GT**. In italics: characteristic times determined experimentally.

5. Conclusions

The combined computational and experimental study presented in this work enriched our knowledge on the excited state relaxation in **GT** and brought further insight on the effect of the DNA polarity on the involved processes.

Differing from the previous *TA* study dedicated to **GT**,[13] our computation of, not only the Franck–Condon states, but also of their relaxation paths, allowed us to identify three minima on the potential energy surfaces of the two most stable conformers. Moreover, the comparison of the **GT** *TAS* with those of dT revealed that the long-lived transient species is not the $^3\pi\pi^*$ triplet of the thymidine chromophore, as hypothesised previously, but the $^1n\pi^*$T state. Thanks to the very high (30 fs) time resolution of our setup, we could follow the stabilization of the ^1CT state, occurring within 120 fs. Thus, we could resolve the dynamics of this process, which was assumed by Duchi *et al.* to be shorter than 350 fs.[13] The striking difference between the **GT** *TAS* at 30 fs and those of an equimolar mixture of dG and dT showed that nucleobases are electronically coupled already in the ground state. Yet, this does not preclude the existence of a minimum located on a single nucleobase, min-$^1\pi\pi^*$G(La). Our conclusions are summarized in a schematic way in Fig. 12.

Regarding the effect of the DNA polarity, the lifetime of the ^1CT state was found to be longer for **GT** (7.48 ± 0.06 ps) compared with that of **TG** (5.44 ± 0.03 ps), studied previously by the same method. The same trend was reported for the **GA**/**AG** pair (170 ps *vs.* 112 ps). It thus appears that the position of the guanine moiety at the 5′ end slows down the ^1CT decay; and it could also contribute to the increase of Φ_{CT}, as judged from the zero-time intensity of the corresponding *TAS*: 26% higher for **GT** with respect to **TG**, and 47% for **GA** with respect to **AG**. However, the determination of absolute Φ_{CT} values remains a challenge. The computation of precise molar absorption coefficients for the ^1CT *TAS*, using higher-level quantum chemistry methods and taking into account vibrational broadening and solvent effects, could contribute to obtaining a more realistic picture.

6. Methods

6.1 Experiments

GT purified by reverse phase HPLC, was purchased by Eurogentec; its purity was tested by MALDI-TOF spectra. The dinucleotide was dissolved in phosphate buffer (0.12 mol L⁻¹, pH 7.0) using Milli-Q water. The purity of the mono-nucleosides and the buffer ingredients (Sigma Alrdrich) was higher than 99.99%. All measurements were performed at room temperature. The molar absorption coefficients reported in Fig. 1a are those provided by Eurogentec.

Steady-state absorption and CD spectra were recorded by means of a PerkinElmer Lambda 1050 spectrophotometer and a JASCO J-815 CD spectrometer, respectively.

TA experiments were conducted using an amplified Ti:Sapphire laser (800 nm, 100 fs pulse duration, 1 kHz repetition rate).[63] Initially, a portion of the laser beam was frequency-doubled to drive a non-collinear optical parametric amplifier (NOPA), generating broadband visible pulses. These pulses were then compressed by chirped dielectric mirrors. Subsequently, the compressed pulses were frequency-doubled in a 20-μm-thick β-barium borate crystal to create broadband UV pump pulses, tunable across the 250–300 nm range. The UV pump pulses were characterized by two-dimensional spectral interferometry and compressed to 24 fs (FWHM) with the aid of a prism pair before being tuned to 266 nm for the experiment. To generate broadband probe pulses, a portion of the primary laser beam was focused onto a 2-mm-thick CaF₂ plate, producing a white-light continuum that spanned from 330 nm to 650 nm. The pump and probe pulses were then non-collinearly focused onto the sample, with spot sizes of 180 μm and 95 μm, respectively. Their relative polarizations were adjusted to the magic angle (54.7°). The pump fluence was maintained at 100 μJ cm⁻², ensuring that the DA signals remained below 10⁻³. This approach effectively minimized contributions from coherent processes and solvated electrons resulting from two-photon ionization of the solvent. During the experiment, a 6 mL solution was continuously flowing through a 1-mm-thick quartz cell using a peristaltic pump.

The instrumental response function (IRF) of the setup was determined from the rise of the stimulated emission (*SE*) signal of the $^1\pi\pi^*$ state of dT, measured under identical experimental conditions as those used for **GT**.[16] It was defined as the time needed for the *SE* intensity to increase from 10% to 90% and found to be 27 fs (Fig. 13). This method captures both the cross-correlation of the pump and probe pulses and any additional broadening due to residual dispersion and group velocity mismatch. The observation of coherent oscillations with periods as short as 42 fs (*e.g.*, the 750 cm⁻¹ mode of dT; Fig. 13) further confirms the ability to resolve ultrafast sub-50 fs dynamics.

The IRF is accounted for in the global analysis of the *TA* data *via* convolution with a kinetic model. In the fitting of the *SE* dynamics of dT, the IRF was treated as a free parameter and was estimated to be a Gaussian function with a FWHM of 28 fs, consistent with the independent 27 fs estimation based on the
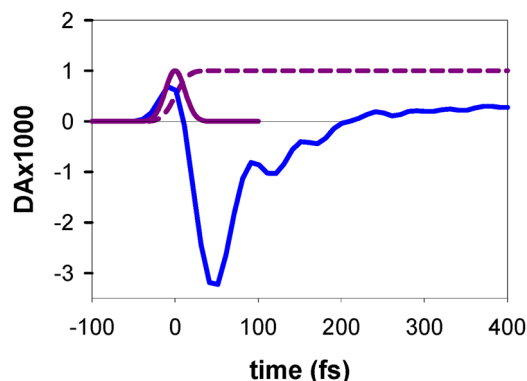
14944 | *Phys. Chem. Chem. Phys.*, 2025, **27**, 14936–14947

This journal is © the Owner Societies 2025

Fig. 13 *TA* dynamics of dT at 335 nm (blue) together with the IRF extracted from fitting procedures (FWHM = 28 fs; violet); the violet dashed line corresponds to the normalized cumulative integral of the IRF.

10–90% rise time. This IRF profile was then used as a fixed parameter in all fits for the **GT** dataset. This approach ensures that all extracted kinetic parameters are corrected for the finite temporal resolution of the setup.

6.2 Computations

Quantum mechanical (QM) calculations were based on the density functional theory (DFT), and its time dependent (TD-DFT) version, using the M052X functional,[64,65] the 6-31G(d) basis set. One Na^+ ion was considered per dinucleotide. The solvent effect was taken into account using an implicit polarizable continuum model (PCM).[66] This method is known to provide accurate results when optimizing charged species and computing spectral properties and *PES* in various DNA systems.[5,67,68]

The vertical absorption energies, intensities (oscillator and rotatory strengths) of the different excited states and the corresponding *PES* were characterized by the above-described methodologies, but resorting to TD-DFT. The *CT* character was computed by a simple Mulliken population analysis in terms of δq, *i.e.*, the difference between the charges in the excited state and in the ground state. All these calculations were done with the Gaussian16 program.[69]

A multifunctional analyser (multiwfn program)[70] provided the transition dipole moments between the excited states for the computation of the *TAS*.

Author contributions

Conceptualization: LMF, GC, DM; data curation: VP, LMF; formal analysis: VP, LMF, EB, DM; funding acquisition: GC, MM, DM; investigation: VP, LMF, LU; methodology: LMF, GC, MM; supervision: GC, MM; validation: all authors; visualization: VP, LMF, EB, DM; writing original draft: VP, LMF, DM; writing – review & editing: VP, LMF, GC, EB, DM.

Conflicts of interest

There are no conflicts to declare.

Data availability

Data are available on https://doi.org/10.5281/zenodo.14938202.

Acknowledgements

References

1 C. Helene and A. M. Michelson, *Biochim. Biophys. Acta*, 1967, **142**, 12–142.

2 J. Eisinger, M. Gueron, R. G. Shulman and T. Yamane, *Proc. Natl. Acad. Sci. U. S. A.*, 1966, **55**, 1015–1020.

3 P. R. Callis, *Chem. Phys. Lett.*, 1973, **19**, 551–555.

4 R. W. Wilson and P. R. Callis, *J. Phys. Chem.*, 1976, **80**, 2280–2288.

5 L. Martinez-Fernandez, F. Santoro and R. Improta, *Acc. Chem. Res.*, 2022, **55**, 2077–2087.

6 V. A. Spata, W. Lee and S. Matsika, *J. Phys. Chem. Lett.*, 2016, **7**, 976–984.

7 F. Plasser and H. Lischka, *Photochem. Photobiol. Sci.*, 2013, **12**, 1440–1452.

8 L. Ibele, P. Sánchez-Murcia, S. Mai, J. Nogueira and L. González, *J. Phys. Chem. Lett.*, 2020, **11**, 7483–7488.

9 A. Francés-Monerris, H. Gattuso, D. Roca-Sanjuán, I. Tuñón, M. Marazzi, E. Dumont and A. Monari, *Chem. Sci.*, 2018, **9**, 7902–7911.

10 L. Martinez Fernandez and R. Improrta, in *Nucleic Acids Photophysics and Photochemistry*, ed. S. Matsika and A. H. Marcus, Springer Nature, 2024, ch. 2, vol. 36, pp. 29–50.

11 T. Takaya, C. Su, K. de La Harpe, C. E. Crespo-Hernandez and B. Kohler, *Proc. Natl. Acad. Sci. U. S. A.*, 2008, **105**, 10285–10290.

12 M. C. Stuhldreier and F. Temps, *Faraday Discuss.*, 2013, **163**, 173–188.

13 M. Duchi, M. P. O'Hagan, R. Kumar, S. J. Bennie, M. C. Galan, B. F. E. Curchod and T. A. A. Oliver, *Phys. Chem. Chem. Phys.*, 2019, **21**, 14407–14417.

14 C. L. Kufner, W. Zinth and D. B. Bucher, *ChemBioChem*, 2020, **21**, 2306–2310.

This journal is © the Owner Societies 2025

Phys. Chem. Chem. Phys., 2025, **27**, 14936–14947 | **14945**

15 V. Petropoulos, L. Uboldi, M. Maiuri, G. Cerullo, L. Martinez-Fernandez, E. Balanikas and D. Markovitsi, *J. Phys. Chem. Lett.*, 2023, **14**, 10219–10224.

16 V. Petropoulos, L. Martinez-Fernandez, L. Uboldi, M. Maiuri, G. Cerullo, E. Balanikas and D. Markovitsi, *Chem. Sci.*, 2024, **15**, 12098–12107.

17 V. Petropoulos, L. Martinez-Fernandez, L. Uboldi, M. Maiuri, G. Cerullo, E. Balanikas and D. Markovitsi, *Biomolecules*, 2024, **14**, 1548.

18 B. Alberts, A. Johnson, J. Lewis, M. Raff, K. Roberts and P. Walter, *Molecular biology of the cell*, Garland Science, New York, 4th edn, 2002, 1548.

19 P. Hazel, J. Huppert, S. Balasubramanian and S. Neidle, *J. Am. Chem. Soc.*, 2004, **126**, 16405–16415.

20 A. Bansal, M. Prasad, K. Roy and S. Kukreti, *Biopolymers*, 2012, **97**, 950–962.

21 P. Sket, T. Korbar and J. Plavec, *J. Mol. Struct.*, 2014, **1075**, 49–52.

22 R. C. Gupta, E. I. Golub, M. S. Wold and C. M. Radding, *Proc. Natl. Acad. Sci. U. S. A.*, 1998, **95**, 9843–9848.

23 W. L. de Laat, E. Appeldoorn, K. Sugasawa, E. Weterings, N. G. J. Jaspers and J. H. J. Hoeijmakers, *Genes Dev.*, 1998, **12**, 2598–2609.

24 S. V. Balasingham, E. D. Zegeye, H. Homberset, M. L. Rossi, J. K. Laerdahl, V. A. Bohr and T. Tonjum, *PLoS One*, 2012, **7**, e36960.

25 Y. H. Lin, C. C. Chu, H. F. Fan, P. Y. Wang, M. M. Cox and H. W. Li, *Nucleic Acids Res.*, 2019, **47**, 5126–5140.

26 I. Saito, M. Takayama, H. Sugiyama and K. Nakatani, *J. Am. Chem. Soc.*, 1995, **117**, 6406–6407.

27 A. Virgilio, V. Esposito, P. Lejault, D. Monchaud and A. Galeone, *Int. J. Biol. Macromol.*, 2020, **151**, 976–983.

28 Y. W. Cao, W. J. Li and R. J. Pei, *ACS Macro Lett.*, 2021, **10**, 1359–1364.

29 M. A. O'Neill and J. K. Barton, *Proc. Natl. Acad. Sci. U. S. A.*, 2002, **99**, 16543–16550.

30 A. A. Voityuk, J. Jortner, M. Bixon and N. Rösch, *J. Chem. Phys.*, 2001, **114**, 5614–5620.

31 C. L. Kufner, S. Crucilla, D. Ding, P. Stadlbauer, J. Sponer, J. W. Szostak, D. D. Sasselov and R. Szabla, *Chem. Sci.*, 2023, 2158–2166.

32 E. Balanikas, L. Martinez-Fernandez, R. Improta, P. Podbevsek, G. Baldacchino and D. Markovitsi, *J. Phys. Chem. Lett.*, 2021, **12**, 8309–8313.

33 A. J. A. Aquino, D. Nachtigallova, P. Hobza, D. G. Truhlar, C. Hattig and H. Lischka, *J. Comput. Chem.*, 2011, **32**, 1217–1227.

34 F. Santoro, V. Barone, A. Lami and R. Improta, *Phys. Chem. Chem. Phys.*, 2010, **12**, 4934–4948.

35 T. Gustavsson and D. Markovitsi, *J. Phys. Chem. Lett.*, 2023, **14**, 2141–2147.

36 D. Onidas, D. Markovitsi, S. Marguet, A. Sharonov and T. Gustavsson, *J. Phys. Chem. B*, 2002, **106**, 11367–11374.

37 W. M. Kwok, C. Ma and D. L. Phillips, *J. Am. Chem. Soc.*, 2008, **130**, 5131–5139.

38 A. Hanes, Y. Y. Zhang and B. Kohler, in *DNA PHOTODAM-AGE: From Light Absorption to Cellular Responses and Skin Cancer*, ed. R. Improta and T. Douki, 2022, vol. 21, pp. 77–104.

39 B. Bouvier, T. Gustavsson, D. Markovitsi and P. Millié, *Chem. Phys.*, 2002, **275**, 75–92.

40 F. Plasser, A. Aquino, H. Lischka and D. Nachtigallová, *Top. Curr. Chem.*, 2015, **356**, 1–38.

41 D. Varsano, R. Di Felice, M. A. L. Marques and A. Rubio, *J. Phys. Chem. B*, 2006, **110**, 7129–7138.

42 J. M. Drake and J. Klafter, *Phys. Today*, 1990, **43**, 46–55.

43 M. F. Shlessinger and A. W. Montroll, *Proc. Natl. Acad. Sci. U. S. A.*, 1984, **81**, 1280–1283.

44 J. M. Drake, J. Klafter and P. Levitz, *Science*, 1991, **251**, 1574–1579.

45 I. Vayá, T. Gustavsson, T. Douki, Y. Berlin and D. Markovitsi, *J. Am. Chem. Soc.*, 2012, **134**, 11366–11368.

46 C. Salet, R. Bensasson and R. S. Becker, *Photochem. Photobiol.*, 1979, **30**, 325–329.

47 B. Amand and R. Bensasson, *Chem. Phys. Lett.*, 1975, **34**, 44–48.

48 S. Marguet and D. Markovitsi, *J. Am. Chem. Soc.*, 2005, **127**, 5780–5781.

49 I. G. Gut, P. D. Wood and R. W. Redmond, *J. Am. Chem. Soc.*, 1996, **118**, 2366–2373.

50 B. M. Pilles, B. Maerz, J. Q. Chen, D. B. Bucher, P. Gilch, B. Kohler, W. Zinth, B. P. Fingerhut and W. J. Schreier, *J. Phys. Chem. A*, 2018, **122**, 4819–4828.

51 A. J. Pepino, J. Segarra-Marti, A. Nenov, I. Rivalta, R. Improta and M. Garavelli, *Phys. Chem. Chem. Phys.*, 2018, **20**, 6877–6890.

52 F. Torche and J. L. Marignier, *J. Phys. Chem. B*, 2016, **120**, 7201–7206.

53 P. M. Hare, C. Crespo-Hernández and B. Kohler, *Proc. Natl. Acad. Sci. U. S. A.*, 2007, **104**, 435–440.

54 Y. Obara, S. Ghosh, A. Humeniuk, S. Kamibashira, S. Adachi and T. Suzuki, *J. Am. Chem. Soc.*, 2025, **147**, 15077–15087.

55 C. C.-W. Cheng, C. Ma, C. T.-L. Chan, K. Y.-F. Ho and W.-M. Kwok, *Photochem. Photobiol. Sci.*, 2013, **12**, 1351–1365.

56 L. Biemann, S. A. Kovalenko, K. Kleinermanns, R. Mahrwald, M. Markert and R. Improta, *J. Am. Chem. Soc.*, 2011, **133**, 19664–19667.

57 S. E. Krul, S. J. Hoehn, K. J. Feierabend and C. E. Crespo-Hernández, *J. Chem. Phys.*, 2021, **154**, 075103.

58 V. Karunakaran, K. Kleinermanns, R. Improta and S. A. Kovalenko, *J. Am. Chem. Soc.*, 2009, **131**, 5839–5850.

59 D. H. Wang, X. L. Wang, Y. R. Jiang, S. M. Cao, P. P. Jin, H. F. Pan, H. T. Sun, Z. R. Sun and J. Q. Chen, *Photochem. Photobiol.*, 2022, **98**, 1008–1016.

60 L. P. Candeias and S. Steenken, *J. Am. Chem. Soc.*, 1992, **114**, 699–704.

61 R. Yamagami, K. Kobayashi and S. Tagawa, *J. Am. Chem. Soc.*, 2008, **130**, 14772–14777.

62 J. Ortín-Fernández, J. González-Vázquez, L. Martínez-Fernández and I. Corral, *Molecules*, 2022, **27**, 989.

63 R. Borrego-Varillas, L. Ganzer, G. Cerullo and C. Manzoni, *Appl. Sci.*, 2018, **8**, 989.

64 Y. Zhao, N. E. Schultz and D. G. Truhlar, *J. Chem. Theory Comput.*, 2006, **2**, 364–382.

14946 | *Phys. Chem. Chem. Phys.*, 2025, **27**, 14936–14947

This journal is © the Owner Societies 2025

65 Y. Zhao and D. G. Truhlar, *Acc. Chem. Res.*, 2008, **41**, 157–167.

66 J. Tomasi, B. Mennucci and R. Cammi, *Chem. Rev.*, 2005, **105**, 2999–3093.

67 R. Improta, F. Santoro and L. Blancafort, *Chem. Rev.*, 2016, **116**, 3540–3593.

68 L. Martinez-Fernandez, L. Esposito and R. Improta, *Photochem. Photobiol. Sci.*, 2020, **19**, 436–444.

69 M. J. Frisch, G. W. Trucks, H. B. Schlegel, G. E. Scuseria, M. A. Robb, J. R. Cheeseman, G. Scalmani, V. Barone, G. A. Petersson, H. Nakatsuji, X. Li, M. Caricato, A. V. Marenich, J. Bloino, B. G. Janesko, R. Gomperts, B. Mennucci, H. P. Hratchian, J. V. Ortiz, A. F. Izmaylov, J. L. Sonnenberg, D. Williams-Young, F. Ding, F. Lipparini, F. Egidi, J. Goings, B. Peng, A. Petrone, T. Henderson, D. Ranasinghe, V. G. Zakrzewski, J. Gao, N. Rega, G. Zheng, W. Liang, M. Hada, M. Ehara, K. Toyota, R. Fukuda, J. Hasegawa, M. Ishida, T. Nakajima, Y. Honda, O. Kitao, H. Nakai, T. Vreven, K. Throssell, J. A. Montgomery, Jr., J. E. Peralta, F. Ogliaro, M. J. Bearpark, J. J. Heyd, E. N. Brothers, K. N. Kudin, V. N. Staroverov, T. A. Keith, R. Kobayashi, J. Normand, K. Raghavachari, A. P. Rendell, J. C. Burant, S. S. Iyengar, J. Tomasi, M. Cossi, J. M. Millam, M. Klene, C. Adamo, R. Cammi, J. W. Ochterski, R. L. Martin, K. Morokuma, O. Farkas, J. B. Foresman and D. J. Fox, *Gaussian 09, revision A.02*, Gaussian Inc., Wallingford, CT, 2016.

70 T. Lu and F. W. Chen, *J. Comput. Chem.*, 2012, **33**, 580–592.

This journal is © the Owner Societies 2025

Phys. Chem. Chem. Phys., 2025, **27**, 14936–14947 | **14947**